Biocatalysis and Agricultural Biotechnology 21 (2019) 101296

Contents lists available at ScienceDirect

Biocatalysis and Agricultural Biotechnology

journal homepage: http://www.elsevier.com/locate/bab

Spiny amaranth leaf extract mediated iron oxide nanoparticles: Biocidal photocatalytic propensity, stability, dissolubility and reusability

M. Harshiny [a,b], S. AiswaryaDevi [a], M. Matheswaran [a,*]

[a] Department of Chemical Engineering, National Institute of Technology, Tiruchirappalli, 620015, India
[b] Applied and Industrial Microbiology Lab, Department of Biotechnology, Indian Institute of Technology Madras, Chennai, 600036, India

ARTICLE INFO

Keywords:
FeO
Biocatalytic
Stability
Cytotoxicity
Antibiofilm
Naphthalene

ABSTRACT

In the recent period, nanomaterial with enhanced multifunctional activity and less mammalian toxicity were greatly required. With this perception, the stability, cytotoxicity and antimicrobial, photocatalytic traits of *Amaranthus spinosus* leaf extract (B-FeO NPs) and sodium borohydride (C-FeO NPs) abridged iron oxide nanoparticles were studied. The analysis results confirmed that B-FeO NPs have better physicochemical characters than C-FeO NPs. The NPs cytotoxicity were tested against MCF-7 cells by MTT assay. The results confirmed that B-FeO NPs cytotoxicity was lesser than C-FeO NPs. The antibacterial and antibiofilm activity of both NPs were tested using *Escherichia coli* and *Bacillus cereus*. The outcomes depicted that synthesized NPs have good inclination against *E. coli* than *B. cereus* bacteria. The photocatalytic efficiency of NPs was assessed using degradation of naphthalene. The result indicate maximum degradation efficiency of 97% for 40 ppm naphthalene under UV light. These results suggest that B-FeO NPs have better physicochemical traits; also, it can be used as an effective bio-catalytic material in biological Industry.

1. Introduction

The increasing world population and the development of industries discharged an enormous number of poison agents and industrial waste into environment (Gupta et al., 2017). Amid, Naphthalene was one of the highly harmful PAHs also it possesses higher water solubility and noxiousness causes kidney impairment, genetic anomalies and cancer in human beings (Liu et al., 2016). Due to its toxicity; effective removal of PAHs from wastewater are exceedingly essential. Various physical, chemical and biological methods have been applied for removing pollutants (Muthukumar et al., 2017b).

In the current epoch, numerous engineered nanomaterials such as Au, Ag, Cu, Fe, CeO_2, TiO_2, ZnO, and FeO are fabricated using various techniques and utilized as personal care, nano-device, antimicrobial agents, catalyst, paints and agricultural products (Pugazhendhi et al., 2018a; Schröfel et al., 2014; Shanmuganathan et al., 2018). However, NPs were restricted in practical uses, it was mainly due to instance less stability, monodispersity, high solubility, wideband and adverse toxic effect (Gatoo et al., 2014; Kahru and Dubourguier, 2010; Pereira et al., 2015). Also, It usage may causes severe health issues to humans and animals (Jiang et al., 2019). Thus, the finding of novel "nano" material requires destroying the aforesaid drawback. Pantidos et al. reported that biological synthesis altering the chemical nature of the toxic metal NPs and it causes no longer toxicity as well as easy to synthesize (Pantidos, 2014). It was reported that plant extracts mediated as Ag, Au, FeO, ZnO NPs synthesis was economically feasible, less toxic extensively used in many field (Iravani, 2011; Pugazhendhi et al., 2018b).

Among the NPs, Iron oxide (FeO) NPs was one of the exceptional materials for environmental to biomedical applications; owing to its fine band gap, chemical constancy, magnetic properties and so on (Mohapatra and Anand, 2011; Muthukumar et al., 2017a). The FeO NPs have numerous usages in the area of cosmetics, bioproducts, bio remediation, medical, materials and manufacturing (El-Kassas et al., 2016; Pereira et al., 2015). It have been reported that green synthesis of Fe NPs was stable, environmentally harmless and demonstrated good cytotoxic properties, antimicrobial activity also act as good photocatalysts for the degradation of azo dye (Alshehri et al., 2017; Kiruba Daniel et al., 2013; Namvar et al., 2014). Previously it was demonstrated that the cost-effective and ecological leaf extract from *Amaranthus* species was an alternative reducing agent for synthesizing NPs (Muthukumar and Matheswaran, 2015). The iron oxide NPs synthesized using leaf extract exposed improved photocatalytic and antioxidant activity than sodium

* Corresponding author.
E-mail address: matheswaran@nitt.edu (M. Matheswaran).

https://doi.org/10.1016/j.bcab.2019.101296
Received 16 May 2019; Received in revised form 14 August 2019; Accepted 19 August 2019
Available online 21 August 2019

borohydride mediated NPs reported in earlier studies (Harshiny et al., 2015). To identify toxic properties of nanomaterials before exposure to humans and the environment might be helpful to improve material and bio- safety (Nel et al., 2010). With this perception, bio-extract mediated iron oxide NPs (B-FeO NPs) were prepared using *A. spinosus* leaf extract. Physicochemical traits, photocatalytic and antioxidant capacity of the B-FeO NPs and sodium borohydride intermediated iron oxide nanoparticles (C-FeO NPs) were reported in prior article (Muthukumar and Matheswaran, 2015).

To further confirms multifunctional activity of B-FeO NPs: size, morphology, composition, dissolubility and stability were examined using various analytical techniques in continuation with previous articles, Also, the photocatalytic degradation efficacy of B-FeO and C-FeO NPs were evaluated using naphthalene under UV irradiation. Before that, B-FeO and C-FeO NPs were tested against MCF-7 cells for cytotoxicity by MTT (3-(4, 5-dimethylthiazolyl-2)-2, 5-diphenyltetrazolium bromide) assay. The antibacterial activity of B-FeO and C-FeO NPs were investigated on *Escherichia coli* (MTCC 7410) and *Bacillus cereus* (MTCC 1272) using disc diffusion method, Minimum inhibitory concentration (MIC), growth kinetics. The crystal violet assay was performed in the existence of B-FeO NPs for observing the biofilm reduction.

2. Experimental section

2.1. Stabilization

Synthesis and Characterization of B-FeO and C-FeO NPs conferred in section S.1.1 and 1.2. (see supplementary material). The steadiness of the NPs was investigated by measuring the zeta potential as well as particle size using SZ-100 nanopartica (Hiroba USA) over time span of 15 days, 1 and 2 months. Prior to stability analysis, the samples were dispersed in pH 7 ± 0.2 deionized water. Tests were performed in triplicates also the results were plotted as mean value ± standard deviation. In addition to this, depending on NPs size (diameter), surface structure and accumulation state of particles influence the band gap (Wang et al., 2014). Thus, the UV–Vis spectrum of B-FeO and C-FeO NPs were measured in the wavelength range from 200 to 800 nm for calculating band-gap stability from absorbance spectrum using tauc plot (Anandalakshmi et al., 2016).

2.2. Dissolubility of NPs in aqueous medium

The dissolubility of NPs was determined by using inductively coupled plasma mass spectrometry (ICP-OES). The concentration of 0.01 g/L NPs in Milli Q water (pH 7 ± 0.2) was taken in an Erlenmeyer flask and agitated for 15mins and the NPs was set aside at 150 rpm in a shaker. At regular interval of time 5 mL of the sample was collected and centrifuged for 10 min at 5000 rpm. The sample was filtered and tested the supernatant for NPs dissolubility (Xia et al., 2011).

2.3. Cell viability assay

Before exploiting the NPs in biological and biomedical application, the quantitative evaluation of B-FeO and C-FeO NP's toxicity was essential. The cell cytotoxicity of B-FeO and C-FeO NPs against MCF-7 cells was found by MTT assay. Around 5×10^3 cells were seeded in microplate (96-well); then cells were treated with various concentrations of NPs for 48 h. After treatment, spent media was cleared from every well and subsequently replenished with new media (DMEM) accompanied with 10 µL (concentration-500 µg/mL) of MTT ((3-(4,5-dimethylthiazol-2-yl) -2,5-diphenyltetrazolium bromide)). The cells were incubated at 37 °C for 3–4 h in due course of which metabolically active, viable cells convert MTT to insoluble formazan crystals. The resulting dark-blue formazan crystals were solubilized in dimethyl sulfoxide (DMSO) and each well was recorded at 574 nm for by Cytation 3 multimode plate reader (Sukumar and Packirisamy, 2015). The obtained absorbance data were denoted as percentage viable cells with respect to untreated cells by the following equation (1);

$$\% \text{ Cell viability} = (A_{574} \text{ in a treated sample}/A_{574} \text{ in control sample}) \text{ X } 100 \quad (1)$$

All experimentations were tested out in triplicates also results were plotted as mean ± SD.

2.4. Cell imaging

In order to monitor events of nuclear fragmentation, a characteristic event of apoptosis, treated cells were blemished with Hoechst 33342 and later investigated by fluorescent microscope. Around 2×10^5 MCF cells were seeded over cover slip in a 3 cm petri plate and treated with NPs for 48 h. After 48 h, the spent media was aspirated gradually and replaced with 2 mL PBS supplemented with 2 µL of Hoechst 33342 dyes (10 mg mL^{-1}) and incubated for 10 min. The staining solution was then replaced with 2% glutaraldehyde cell fixative solution and allowed to stand for 5 min (Sachdev and Gopinath, 2015). The glutaraldehyde solution was eliminated and the fixed cells were briefly washed with gradient solution of ethanol. The morphology of treated cells was visualized and captured by EVOS FL Cell Imaging System under DAPI filter and transmitted mode. The antibacterial activities of B-FeO and C-FeO NPs were carried out by disc diffusion, MIC, growth curve study and antibiofilm activities against *E. coli* and *B. cereus* were performed and procedures were given in section S.1.3 to S.1.6. (see supplementary material).

2.5. Photocatalytic activity

The photocatalytic degradation efficiency of B-FeO and C-FeO NPs after 60 days from synthesis was measured by naphthalene degradation under UV light irradiation. The Photocatalytic activity studies were performed in a double jacket cylindrical container with circulation of cooling water for retaining the study temperature. The photocatalytic reactor with UV light of 16 W was positioned on a magnetic stirrer. 750 mL of naphthalene solution was poured in the reactor and NPs were added. Above solution was uninterruptedly showing to UV light maintained at 37 ± 1 °C for 150 min. The samples were taken out at a consistent time interval and before analysis the photocatalyst was filtered. The degradation percentage was measured using UV–visible spectrophotometer with a wavelength range of 200–700 nm (Muthukumar et al., 2017b). The percentage of photocatalytic degradation efficiency of NPs was calculated using the following equation,

$$\text{Percentage of degradation} = (A_0\text{-}A_t)/A_0 * 100$$

Where A_0 and A_t is initial concentration and after the time ('t') of naphthalene solution absorbance.

3. Result and discussion

3.1. Characterization of NPs using analytical techniques

The XPS spectrum of B-FeO and C-FeO NPs were shown in Fig. 1. The B-FeO NPs photoelectron profiles evidently confirm the peaks of 530.4 eV are attributed to O 1s and O may arise from the iron oxide lattice of bio molecules and water (Makarov et al., 2014). The C 1s signal at 286.4 was mainly from C atoms in the polyphenol groups bind to NPs. In particular, the survey of Fe core levels was observed at 709.5 eV, 711.4 eV and 725.2 eV; represent the binding energies of 2p3/2 and 2p1/2 electrons respectively. As well, Shahwan et al. synthesized green tea extracts mediated iron NPs, also observed similar binding energies of Fe 2p3/2 and 2p1/2 from iron oxide and iron-oxohydroxide (Shahwan et al., 2011). In addition to Fe and O, photoelectron lines NPs displayed low intensity peaks of Na and Cl, these electrons may possibly from Fe precursor and reactant. Likewise, the XPS spectrum of C-FeO NPs also

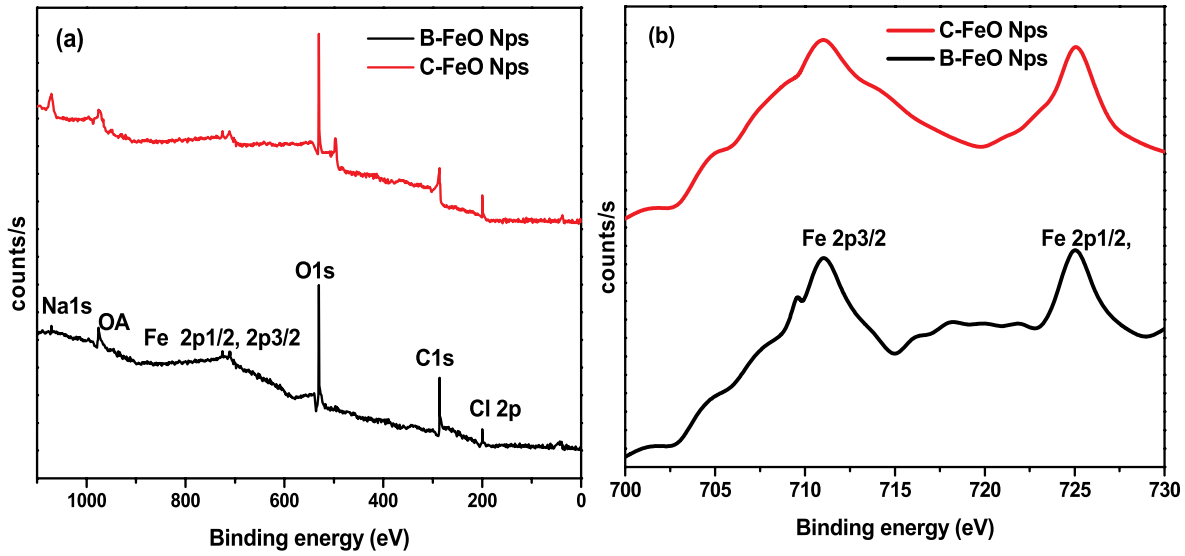

Fig. 1. The XPS survey spectrum (a) and Fe2P XPS spectra of B-FeO and C-FeO NPs (b).

showed carbon C 1s, oxygen O 1s and iron Fe 2p binding energy. The results show the presence of higher organic molecules and FeO in the synthesized samples. It strongly believed that B-FeO NPs are going play an vital role in constancy and applications. Fig. S1 (see supplementary) shows CIE colour coordinate diagram and PL emission spectra of C-FeO and B-FeO NPs; as well as it explanation was given in S.2.1. (see supplementary).

The B-FeO and C-FeO NPs morphology were investigated using SEM; Fig. 2a apparently depicted mono-dispersed micrograph of B-FeO NPs. In contrast, Fig. 2b of C-FeO NPs was aggregated. It was noted that B-FeO and C-FeO NPs were appeared to hold like a spherical morphology. The SEM micrograph further reconfirm that B-FeO have better morphology, stability and less accumulation owed to organic compounds acting as capping agents. Therefore, B-FeO NPs were expected to be helpful for ample biological applications (Venkateswarlu et al., 2013).

3.2. Stability and dissolubility of NPs

The B-FeO and C-FeO NPs stability were assessed using UV–Vis spectrum, particle size and zeta potential analysis for the period of 3, 15, 30 and 60 days after synthesis. The NPs absorbance, potential and size distribution varied dependent on morphology, band gap and accumulation state, through its modification FeO NPs stability was easily evaluated (Amendola and Meneghetti, 2009). Figs. S2 and S3 (see supplementary) evidently depicts that B-FeO NPs size does not shown significant transformation up to 15 days, but NPs average size increased from 92.5 to 94.8 and 96.2 nm over a period of 1 and 2 month. It was owed to organic compounds in the leaf extract, acting as capping agents to avoid NPs aggregation and improve NPs colloidal suspension stabilization (Muthukumar and Matheswaran, 2015). In contrast C-FeO NPs profusely increased from 125 to 136 nm after synthesis of 15, 30 and 60 days respectively. The occurrence of variations in C-FeO NPs may due to storage without capping/stabilization agent, nature of material, environmental factor.

Accordingly, the B-FeO NPs band-gap was calculated using tauc plot. Fig. S2 (see supplementary) illustrated that the band energy of 2eV on the 15th day and it was slightly changed to 2.12 and 2.18 eV after 30 and 60 days respectively. As well as for C-FeO NPs band gap increased 2.35 to 2.5 and 2.62 eV were calculated. The zeta potential range was observed from 65 to 60.5 mV and 45 to 42 mV, for B-FeO and C-FeO respectively. Fig. S2 apparently illustrates that the optical band gap energy decreases with increase in NPs size. Additionally, NPs stability was confirmed using ICP-OES investigation, the result confirmed that up to 100 h in Milli Q water does not display the Fe content for B-FeO and C-FeO NPs. DMSO Dissolved, water dispersed and settled observation of B-FeO and C- FeO NPs were shown in Fig. S4 (see supplementary). It confirmed that B-FeO shows lesser amount of solubility in water and holding improved stability. It was owed to organic molecules accumulate on FeO NPs surface and increasing surface charge that enhances NPs

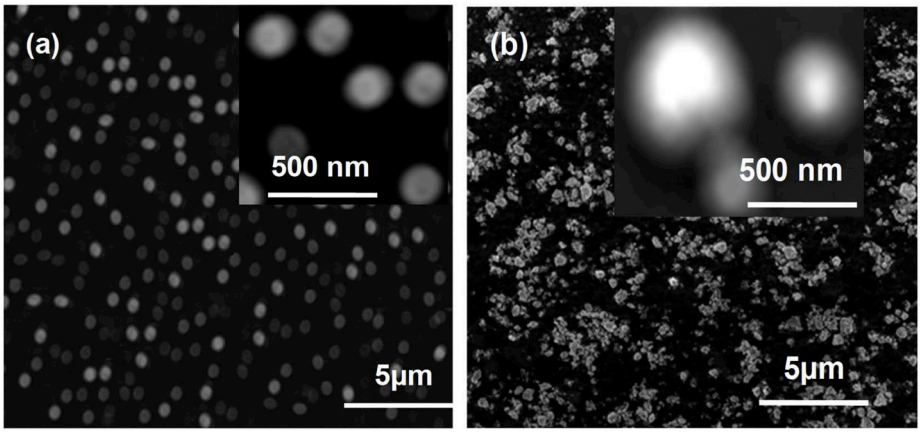

Fig. 2. SEM micrograph of 5 μm magnification (inset: 500 nm magnification) B-FeO(a) and C-FeO NPs(b).

stability by reducing aggregation (Mohapatra and Anand, 2011). In addition, results clearly demonstrate that bio-extract mediated NPs exposed better yield, stability, smaller size, fewer aggregation compared to C-FeO NPs. Thus B-FeO NPs will be applied for safe environmental and clinical applications.

3.3. Cytotoxicity evaluation

The MTT assay was quantitatively evaluated the cytotoxicity of B-FeO, C- FeO NPs at different concentrations in MCF-7 cells. Fig. 3a was clearly evident that, at the concentration of 500 µg/ml, B-FeO NPs treatment manifested 59.92% of cell viability, whereas C-FeO NPs further declined to 53.25%. The IC_{50} values for B-FeO, C- FeO NPs were determined to be 600 and 533 µg/mL, respectively. MTT assay of B-FeO NPs showed >90% viability of cells in lower concentrations (0–100 µg/mL) and whereas at higher concentrations (600–800 µg/mL) viability reduced to 50%–33%. Above the IC_{50} concentration of C-FeO NPs demonstrated increased toxicity than B-FeO NPs. The results, further confirmed that both NPs at higher concentration shows significant MCF cell reduction after 48 h. It indicates that, higher concentration of NPs exposure resulted in enhanced ROS generation. Also, the cell injury and death occurred depends on concentration of NPs (Naqvi et al., 2010). It was reported that high levels of FeO NPs at the aimed site could create a disproportion in homeostasis and cellular responses alteration; leads to DNA damage, oxidative strain, genetic alteration, cytoskeletal organization of cells distraction and cytotoxicity (Wahajuddin, 2012). Further, results have been depicted that B-FeO NPs had no considerable cytotoxic effect. B-FeO and C-FeO shows the less cytotoxicity effect at lower doses up to 250 µg/ml and 100 µg/ml respectively. In accordance, Kanagesan et al. also investigated the FeO NPs cytotoxic effect on MCF-7 breast cancer cells and revealed that higher concentrations of NPs increased to 100, 200 and 400 µg/mL significantly reduced the viability of cells. The result further confirms that C-FeO NPs cytotoxicity was slightly higher than B-FeO NPs (Kanagesan et al., 2013). Such a discrepancy in the results suggests that the biocompatibility or toxicity of NPs dependent on physicochemical, density of functional groups. Composition of chemicals adsorbed onto the surfaces type of reducing agents used for NPs synthesis (S. et al., 2015). The reduced activity of B-FeO NPs may owe to organic molecules from leaf extract encapsulated on the surface have a large number of OH- groups and can complex well through metal ions. When cancer cells uptakes B-FeO NPs and metabolize leads to the reduced toxicity (Vidic et al., 2013). Further, Malvindi et al. stated that surface functionalization of FeO NPs sturdily improve biocompatibility by enhancement of its resistance. Therefore, synthesis method and surface of FeO NPs may change the NPs dissolution kinetics, toxicity decreases and making a nontoxic nanomaterial for biological uses (Malvindi et al., 2014).

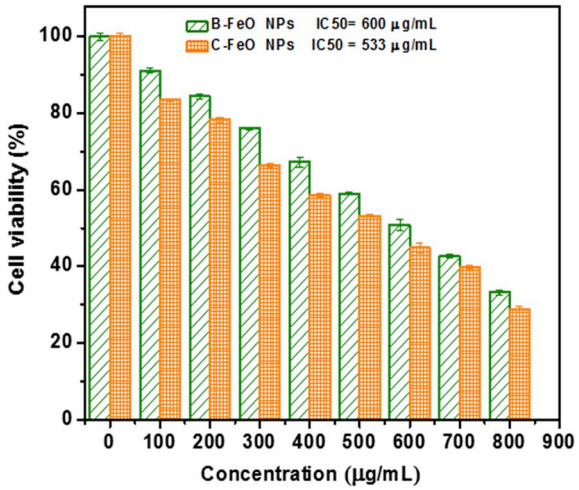

Fig. 3. a.*In vitro* cytotoxicity assay of C-FeO and B-FeO NPs against MCF-7 Cell lines.

3.4. Morphological assessment of MCF-7 cells

B-FeO NPs IC_{50} concentration treated cancer MCF-7 cells were stained with Hoechst 33342 to identify apoptotic cells with spotted nuclear morphology Fig. S5 (see supplementary). The presence of such spotted, bright, non-uniformly stained nucleus confirms fragmentation of nucleus; that characteristic event of apoptosis (Vivek et al., 2012). Such events of apoptosis were evident in case of both NPs, but to different extents (indicated by short white arrows). In contrast to treated cells, control nuclear cell morphology remained intact and distinctly visible as uniformly stained features under DAPI filter. Thus, decline cell viability in MTT assay observed by microscopic observation further confirms that apoptotic cell death mediated by NPs (Suresh et al., 2012). IC_{50} concentration of C-FeO NPs treated MCF-7 Hoechst 33342 stained were shown in Fig. S6 (see supplementary).

3.5. Disc diffusion assay

The different concentrations of 10, 15 and 20 µL B-FeO and C-FeO NPs antimicrobial activity towards *E. coli* and *B. cereus* bacteria were tested by qualitative disc diffusion assay. Table S1 depicts the inhibition zone diameter measurements for B-FeO, C-FeO NPs, streptomycin and leaf extract. It apparently depicted that, the prepared B-FeO NPs have enhanced antibacterial activity than C-FeO and leaf extract as well as, B-FeO NPs showed zone of inhibition equivalent to streptomycin.

Based on the way of synthesis, NPs hold shape distribution, a wide-ranging size and surface charges also variable range of bioactivity (Gatoo et al., 2014). The better activity of B-FeO NPs was owe to biomolecules encapsulated on NPs surface and considerably increases its surface charge, area and active site that improves NPs stability by preventing aggregation than C-FeO NPs (Alshehri et al., 2017). B-FeO NPs higher positive zeta potential holds better surface area; So stronger bacterial attachment leads to interactions at an interface (Alshehri et al., 2017). The high interactions result in comparatively improved ROS production; that cause of NPs antimicrobial propensity also causing oxidative stress to bacterial cells, hence bacterial cell death occurred (Arakha et al., 2015). In addition, the presence of a thick peptidoglycan layer cell wall in Gram + ve bacteria (Kuppusamy et al., 2016). But, a thin layer of peptidoglycan with nanometre range pores and layer of lipopolysaccharide at the outer surface in Gram -ve bacteria (Azam et al., 2012). Owed to, test NPs were maximum effect for *E. coli* Gram -ve bacteria than *B. cereus* Gram + ve bacteria as shown in Fig. 4. Sumathi et al. tried antibacterial and antibiofilm activity of anethole coated FeO NPs against *E. coli, S. aureus, B. subtilus, P. aeroginosa* and *K. Pneumonia*. The anethole coated FeO NPs zone of inhibition were found to be highest of 13 mm (Sampathkumar et al., 2016) It clearly represented that, B-FeO NPs have enhanced antibacterial activity.

3.6. MIC of FeO NPs

Minimum number of NPs required for antimicrobial activity was determined after of test bacteria and NPs incubation at 37 °C for 24 h by the standard MIC method, as shown in Fig. 5. It was apparently depicted that NPs have noticeable bactericidal efficacy on *E.coli* and *B. cereus*; compared to controls. The growth of *E.coli* was inhibited by 93 and 40% in the presence of B-FeO and C-FeO NPs; 60 and 30% of *B. cereus* growth was reduced in the presence of 250 µg/mL B-FeO and C-FeO NPs respectively. However, 250 µg/mL of C-FeO NPs does not show any significant inhibition. These results show a better antimicrobial activity against Gram –ve bacteria at lower concentration of NPs, also showed activity against Gram + ve at higher concentrations of NPs. It was due to, beyond a certain concentration of NPs, the net collaborative interaction

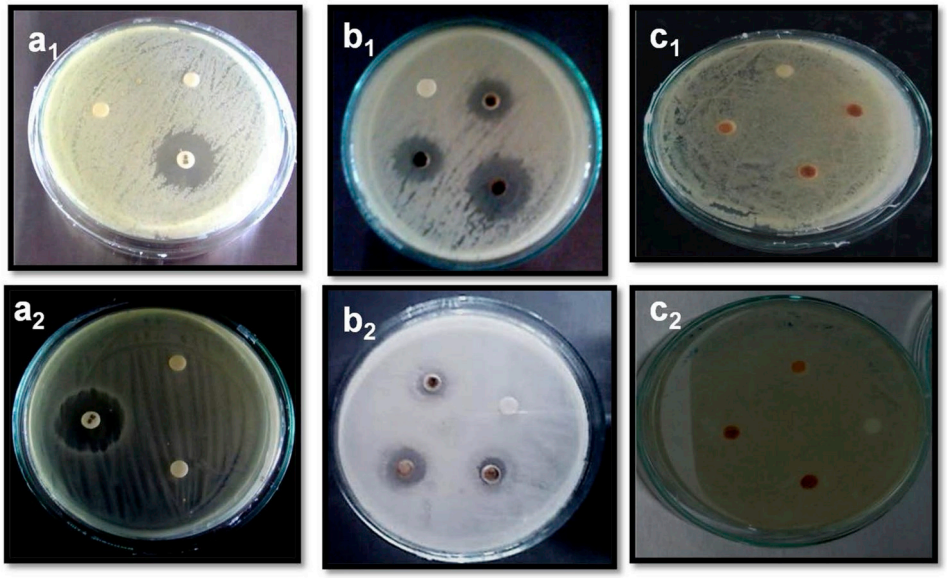

Fig. 4. Inhibition zone measurements of Streptomycin and B-FeO and C-FeO NPs against *E.coli* (a_1,b_1, c_1) and *B. cereus* (a_2,b_2,c_2).

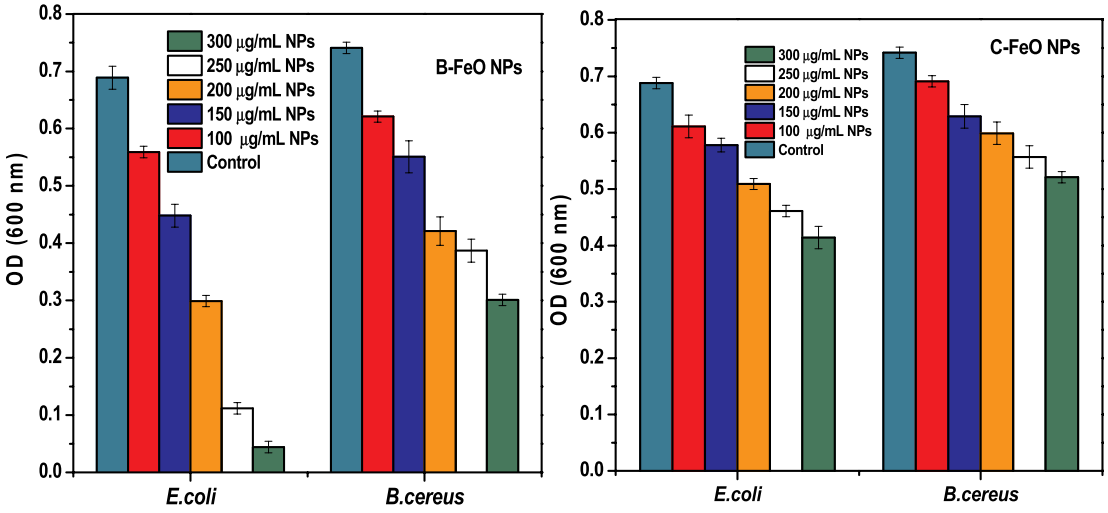

Fig. 5. MIC of B-FeO NPs and C-FeO NPs against *E.coli* and *B. cereus*.

enhances ROS production at the interface (Erik et al., 2012). The optimum MIC was determined to be 250 µg/mL of B-FeO NPs for Gram -ve bacteria. As well as significant decrease of CFUs were observed and it was shown in Fig. S7 (see supplementary); the same concentration of B-FeO NPs does not shows high inhibition for Gram + ve bacteria. Markedly, the MIC of 350 µg/mL B-FeO NPs shows 90% inhibition for Gram + ve bacteria.

3.7. Effect of B-FeO NPs on bacterial growth kinetics

The growth curve study has been done by observing B-FeO treated and untreated *E. coli* and *B. cereus* growth. The control experiment of *E. coli* and *B. cereus* growth curve demonstrates that lag, log, stationery and death phases were closely from 0-4th, 5- 11th, 12th-24th and 27th h. The results also showed that, bacteria growth inhibition was high in the existence of B-FeO NPs compared to devoid of nanoparticles. *E. coli* and *B. cereus* growth was impeded in the early stages; then no noticeable growth after seventh h and it was shown in Fig. 6. At stationary phase propensity of the NPs and control culture was envisaged under microscope. The samples for microscopic imaging procedure reported by Arakha et al. were followed with a little change (Arakha et al., 2015). Fig. 6 depicted viable bacterial cells presence in images by green fluorescence also combination of green and red fluorescence micrograph shows a mix of normal and affected cells. Also, B-FeO NPs treated bacteria cell membrane physical disruption; size reduced and colony count were compared to the control (Khodashenas and Ghorbani, 2015). It was speculated that the B-FeO NPs physicochemical traits promotes NPs, bacterial exchanges by cell membranes and reparations proteins, internal membranes and DNA, leads to decrease in viability (Seil and Webster, 2012). It deceptively showed that, B-FeO NPs have improved antibacterial efficacy.

3.8. Inhibition of biofilms

The inhibition of biofilm formation using various concentrations (100, 200 and 300 µg/mL) of NPs influence against *E. coli* and *B. cereus* were shown in Fig. 7. The biofilm inhibition by B-FeO NPs was observed 89 and 55.5% for *E. coli* and *B. cereus*. The result illustrates that increase in the concentration of B-FeO NPs shows high inhibition of biofilm development. It was due to Fe ions diffusion inside biofilm matrixes by

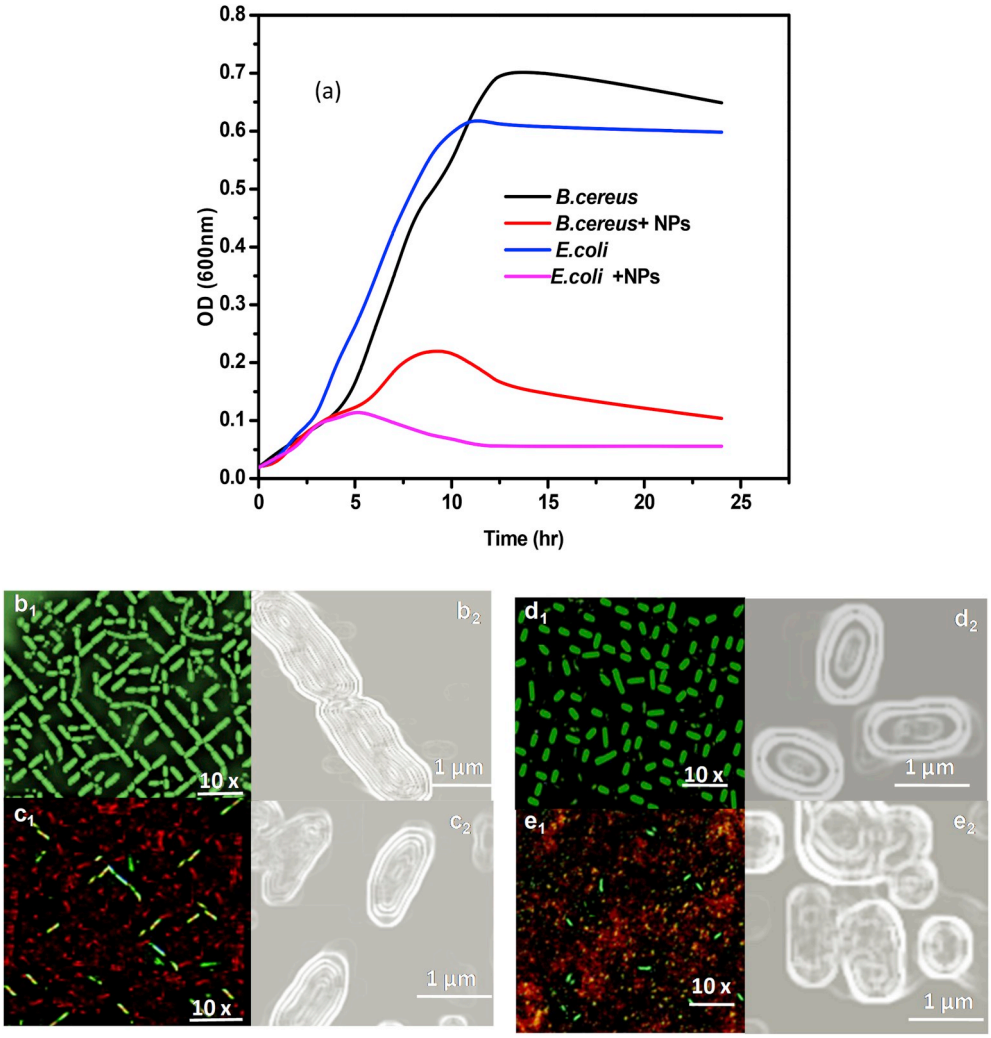

Fig. 6. a.Growth kinetics of Gram + ve and –ve bacteria in the presence and absence of B-FeO NPs.Control *B.cereus* (b1,b2), *E.coli* (d1, d2) and FeO Nps treated *B. cereus* (c1,c2), *E.coli* (e1, e2) microscopic small and higher magnification images.

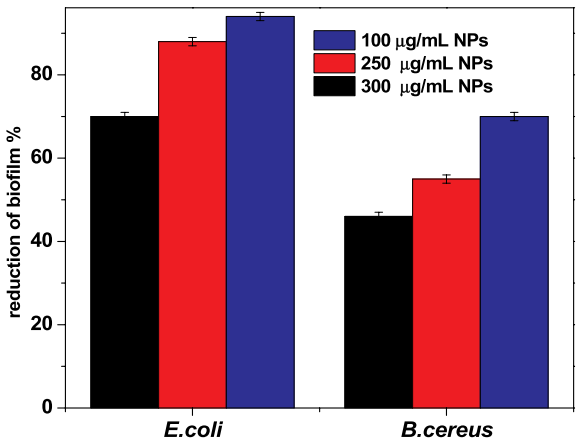

Fig. 7. Percentage reduction of biofilms using B-FeO NPs.

altering surface and can interrupt the cell function by binding to internal proteins and enzymes (Hajipour et al., 2012; Sharma et al., 2015). Ramalingam et al., reported 200 µg/ml of iron oxide NPs after 24 h treatment. *E. coli, P. aeruginosa* and *S. aureus* exopolysaccharide production was inhibited 69%, 65% and 60% (Ramalingam et al., 2019). Hence, biofilm formation by the test bacteria was reduced in presence of B-FeO NPs also shows an enhanced antibacterial activity. Further, investigations are needed to evaluate the impact of straight physical influence and discharge of metal ions from NPs to a bacterial cell.

3.9. Photocatalytic and reusability studies of B-FeO and C-FeO NPs

Photocatalytic activities of B-FeO and C-FeO NPs were examined using 40 ppm of naphthalene at pH 7. As a control experiment, naphthalene degradation has been executed in UV light without a catalyst (photolysis) and with 200mg/750 mL of the catalyst under dark condition (adsorption) for 150 min. Fig. 8 shows the degradation efficiency of the NPs under various experimental parameters. 14% degradation of naphthalene was noticed for photolysis, whereas 200mg/750 mL of B-FeO and C-FeO NPs under dark condition exhibited 35%, 24%, respectively. The degradation efficiency of NPs under dark condition was slightly high; attributed to adsorption of naphthalene on the surface of NPs. Lastly, under UV light naphthalene degradation of 82% and 97% were obtained for C-FeO and B-FeO NPs, respectively. For control, the degradation efficiency of leave extract for 40 ppm naphthalene was observed to be 9 ± 1% at 150 min. Earlier it was reported that higher degradation efficiency of 63.5 and 71.7% was found in the occurrence of *A. dubius* mediated ZnO and Fe-ZnO under UV light irradiation at pH 7 (Muthukumar et al., 2017b). Sekar et, al., reported that under UV light naphthalene degradation of 58 and 70% efficiencies were obtained for

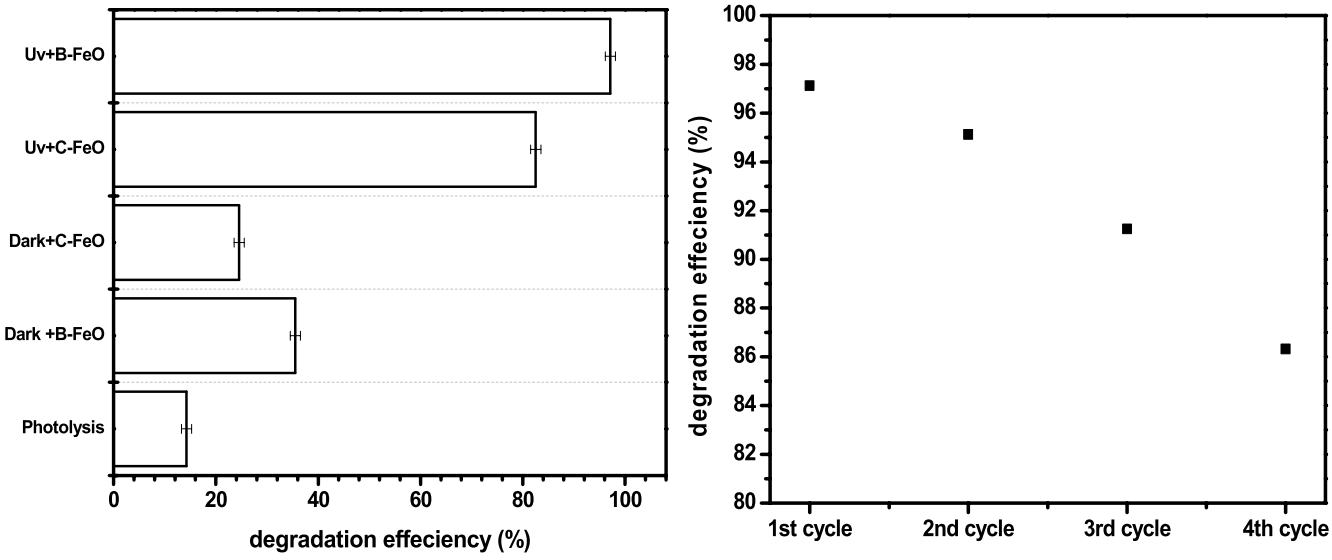

Fig. 8. Photocatalytic degradation of 40 ppm of naphthalene using FeO NPs, under UV light and recyclability studies of NPs for the photocatalytic degradation of naphthalene for up to four cycles.

A. spinosus leaf extract mediated ZnO NPs and Fe-doped ZnO NPs (Sekar et al., 2018). Consequently, the results confirmed that B-FeO NPs showed better degradation efficiency than C-FeO NPs after 60 days from the date of synthesis.

The recyclability of B-FeO NPs was tested for consequent four cycles with the same NPs recovered from the previous experiments and the new naphthalene solution was taken after every cycle. Fig. 8 shows the B-FeO NPs photocatalytic efficiency up to four cycles. Initially, no significant decrease was detected up to three cycles. It was stated that NPs photocatalytic activities depend on physicochemical traits. It also reported that, biomediated NPs have huge number of boundaries so it enhances the transport photoelectron that can develop OH- radical creation and gave an excellent degradation result (Muthukumar and Matheswaran, 2015).

4. Conclusion

Green mediated preparation of stable FeO NPs using leaf extract of *A. spinosus* and $NaBH_4$ was reported in this study. The characterization proves B-FeO NPs holds less particles size, band gap and high stability, monodisperses compared to C-FeO NPs. The synthesized B-FeO NPs exhibited significant antimicrobial activities for *E. coli* and *B.cereus* than C-FeO NPs. The B-FeO NPs optimum MIC was determined to be 250 μg/mL for gram negative bacteria and 350 μg/mL for gram positive bacteria. B-FeO NPs depicted the better biofilm inhibition of 89 and 55.5% for *E.coli* and *B.cereus*. The toxicological impacts of B-FeO NPs were studied and compared to C -FeO NPs against MCF-7 cells. The IC50 values for B-FeO, C- FeO NPs were determined to be 600 and 533 μg/mL, respectively. B-FeO and C-FeO NPs under UV light 97% and 82% of naphthalene degradation were obtained. This result further confirmed *A. spinosus* leaf extracts won't generate any noxious by-products. It can be proposed that leaf extract of *A. spinosus* was a better alternate to noxious reducing products like $NaBH_4$ and B- FeO NPs could be used effectively in bioapplications.

Acknowledgments

The authors M.M are grateful to Department of Science and Technology, Government of India (NO.SB/FT/CS-047/2012) and M.M and M.H Department of Biotechnology (BT/PR6080/GBD/27/503/2013) Government of India for the financial assistance. MH thank Ashish Gire for photocatalytic studies. Dr. J. Sarat Chandra Babu and G. Bhuvaneswari Department of Chemical Engineering, NIT Trichy for Particle Size analysis and ICPOES interpretation. MH acknowledges SERB-DST for the National Post-doctoral fellowship (SO.No:PDF/2018/000795).

Appendix A. Supplementary data

Supplementary data to this article can be found online at https://doi.org/10.1016/j.bcab.2019.101296.

References

Alshehri, A., Malik, M.A., Khan, Z., Al-Thabaiti, S.A., Hasan, N., 2017. Biofabrication of Fe nanoparticles in aqueous extract of Hibiscus sabdariffa with enhanced photocatalytic activities. RSC Adv. 7, 25149–25159. https://doi.org/10.1039/c7ra01251a.

Amendola, V., Meneghetti, M., 2009. Size Evaluation of Gold Nanoparticles by UV - Vis Spectroscopy, pp. 4277–4285.

Anandalakshmi, K., Venugobal, J., Ramasamy, V., 2016. Characterization of silver nanoparticles by green synthesis method using Pedalium murex leaf extract and their antibacterial activity. Appl. Nanosci. 6, 399–408. https://doi.org/10.1007/s13204-015-0449-z.

Arakha, M., Pal, S., Samantarrai, D., Panigrahi, T.K., Mallick, B.C., Pramanik, K., Mallick, B., Jha, S., 2015. Antimicrobial activity of iron oxide nanoparticle upon modulation of nanoparticle-bacteria interface. Sci. Rep. 5, 1–12. https://doi.org/10.1038/srep14813.

Azam, A., Ahmed, A.S., Oves, M., Khan, M.S., Habib, S.S., Memic, A., 2012. Antimicrobial activity of metal oxide nanoparticles against Gram-positive and Gram-negative bacteria: a comparative study. Int. J. Nanomed. 7, 6003–6009. https://doi.org/10.2147/IJN.S35347.

El-Kassas, H.Y., Aly-Eldeen, M.A., Gharib, S.M., 2016. Green synthesis of iron oxide (Fe3O4) nanoparticles using two selected brown seaweeds: characterization and application for lead bioremediation. Acta Oceanol. Sin. 35, 89–98. https://doi.org/10.1007/s13131-016-0880-3.

Erik, N. Taylor, Kummer, Kim M., Naside Gozde Durmus, K.L., Tarquinio, Keiko M., W, T. J., 2012. Superparamagnetic iron oxide nanoparticles (SPION) for the treatment of antibiotic-resistant biofi lms. Small 8, 3016–3027.

Gatoo, M.A., Naseem, S., Arfat, M.Y., Mahmood Dar, A., Qasim, K., Zubair, S., 2014. Physicochemical properties of nanomaterials: implication in associated toxic manifestations. BioMed Res. Int. 2014. https://doi.org/10.1155/2014/498420.

Gupta, H., Kumar, R., Park, H.S., Jeon, B.H., 2017. Photocatalytic efficiency of iron oxide nanoparticles for the degradation of priority pollutant anthracene. Geosyst. Eng. 20, 21–27. https://doi.org/10.1080/12269328.2016.1218302.

Hajipour, M.J., Fromm, K.M., Akbar Ashkarran, A., Jimenez de Aberasturi, D., Larramendi, I.R. de, Rojo, T., Serpooshan, V., Parak, W.J., Mahmoudi, M., 2012. Antibacterial properties of nanoparticles. Trends Biotechnol. 30, 499–511. https://doi.org/10.1016/j.tibtech.2012.06.004.

Harshiny, M., Iswarya, C.N., Matheswaran, M., 2015. Biogenic synthesis of iron nanoparticles using Amaranthus dubius leaf extract as a reducing agent. Powder Technol. 286, 744–749. https://doi.org/10.1016/j.powtec.2015.09.021.

Iravani, S., 2011. Green synthesis of metal nanoparticles using plants. Green Chem. 13, 2638–2650. https://doi.org/10.1039/c1gc15386b.
Jiang, Z., Shan, K., Song, J., Liu, J., Rajendran, S., Pugazhendhi, A., Jacob, J.A., Chen, B., 2019. Toxic effects of magnetic nanoparticles on normal cells and organs. Life Sci. 220, 156–161. https://doi.org/10.1016/j.lfs.2019.01.056.
Kahru, A., Dubourguier, H.C., 2010. From ecotoxicology to nanoecotoxicology. Toxicology 269, 105–119. https://doi.org/10.1016/j.tox.2009.08.016.
Kanagesan, M., Hashim, S., Tamilselvan, N.B., Alitheen, I., Ismail, A., Hajalilou, 1, Ahsanul3, K., 2013. Synthesis, characterization, and cytotoxicity of iron oxide nanoparticles. Adv. Mater. Sci. Eng. 7.
Khodashenas, B., Ghorbani, H.R., 2015. Synthesis of silver nanoparticles with different shapes. Arab. J. Chem. https://doi.org/10.1016/j.arabjc.2014.12.014.
Kiruba Daniel, S.C.G., Vinothini, G., Subramanian, N., Nehru, K., Sivakumar, M., 2013. Biosynthesis of Cu, ZVI, and Ag nanoparticles using Dodonaea viscosa extract for antibacterial activity against human pathogens. J. Nanoparticle Res. 15. https://doi.org/10.1007/s11051-012-1319-1.
Kuppusamy, P., Yusoff, M.M., Maniam, G.P., Govindan, N., 2016. Biosynthesis of metallic nanoparticles using plant derivatives and their new avenues in pharmacological applications – an updated report. Saudi Pharm. J. 24, 473–484. https://doi.org/10.1016/j.jsps.2014.11.013.
Liu, D., Wu, Z., Tian, F., Ye, B.C., Tong, Y., 2016. Synthesis of N and la co-doped TiO2/AC photocatalyst by microwave irradiation for the photocatalytic degradation of naphthalene. J. Alloy. Comp. 676, 489–498. https://doi.org/10.1016/j.jallcom.2016.03.124.
Makarov, V.V., Makarova, S.S., Love, A.J., Sinitsyna, O.V., Dudnik, A.O., Yaminsky, I.V., Taliansky, M.E., Kalinina, N.O., 2014. Biosynthesis of stable iron oxide nanoparticles in aqueous extracts of hordeum vulgare and rumex acetosa plants. Langmuir 30, 5982–5988. https://doi.org/10.1021/la5011924.
Malvindi, M.A., De Matteis, V., Galeone, A., Brunetti, V., Anyfantis, G.C., Athanassiou, A., Cingolani, R., Pompa, P.P., 2014. Toxicity assessment of silica coated iron oxide nanoparticles and biocompatibility improvement by surface engineering. PLoS One 9, 1–11. https://doi.org/10.1371/journal.pone.0085835.
Mohapatra, M., Anand, S., 2011. Synthesis and applications of nano-structured iron oxides/hydroxides – a review. Int. J. Eng. Sci. Technol. 2, 127–146. https://doi.org/10.4314/ijest.v2i8.63846.
Muthukumar, H., Matheswaran, M., 2015. Amaranthus spinosus leaf extract mediated FeO nanoparticles: physicochemical traits, photocatalytic and antioxidant activity. ACS Sustain. Chem. Eng. 3, 3149–3156. https://doi.org/10.1021/acssuschemeng.5b00722.
Muthukumar, H., Chandrasekaran, N.I., Naina Mohammed, S., Pichiah, S., Manickam, M., 2017. Iron oxide nano-material: physicochemical traits and in vitro antibacterial propensity against multidrug resistant bacteria. J. Ind. Eng. Chem. 45, 121–130. https://doi.org/10.1016/j.jiec.2016.09.014.
Muthukumar, H., Gire, A., Kumari, M., Manickam, M., 2017. Biogenic synthesis of nano-biomaterial for toxic naphthalene photocatalytic degradation optimization and kinetics studies. Int. Biodeterior. Biodegrad. 119, 587–594. https://doi.org/10.1016/j.ibiod.2016.10.036.
Namvar, F., Rahman, H.S., Mohamad, R., Baharara, J., Mahdavi, M., Amini, E., Chartrand, M.S., Yeap, S.K., 2014. Cytotoxic effect of magnetic iron oxide nanoparticles synthesized via seaweed aqueous extract. Int. J. Nanomed. 9, 2479–2488. https://doi.org/10.2147/IJN.S59661.
Naqvi, Naqvi, Samim, M., Abdin, M.Z., Ahmad, F.J., prashant, C.K., Dinda, A., 2010. Concentration-dependent toxicity of iron oxide nanoparticles mediated by increased oxidative stress. Int. J. Nanomed. 983. https://doi.org/10.2147/ijn.s13244.
Nel, A.E., George, S., Pokhrel, S., Xia, T., Gilbert, B., Ji, Z.X., Schowalter, M., Rosenauer, A., Damoiseaux, R., Bradley, K.A., Madler, L., 2010. Use of a rapid cytotoxicity screening approach to engineer a safer zinc oxide nanoparticle through iron doping. ACS Nano 4, 15–29. https://doi.org/10.1021/Nn901503q.
Pantidos, N., 2014. Biological synthesis of metallic nanoparticles by bacteria, fungi and plants. J. Nanomed. Nanotechnol. 05. https://doi.org/10.4172/2157-7439.1000233.
Pereira, C., Pereira, A.M., Rocha, M., Freire, C., Geraldes, C.F.G.C., 2015. Architectured design of superparamagnetic Fe_3O_4 nanoparticles for application as MRI contrast agents: mastering size and magnetism for enhanced relaxivity. J. Mater. Chem. B 3, 6261–6273. https://doi.org/10.1039/c5tb00789e.
Pugazhendhi, A., Edison, T.N.J.I., Karuppusamy, I., Kathirvel, B., 2018. Inorganic nanoparticles: a potential cancer therapy for human welfare. Int. J. Pharm. 539, 104–111. https://doi.org/10.1016/j.ijpharm.2018.01.034.
Pugazhendhi, A., Prabakar, D., Jacob, J.M., Karuppusamy, I., Saratale, R.G., 2018. Synthesis and characterization of silver nanoparticles using Gelidium amansii and its antimicrobial property against various pathogenic bacteria. Microb. Pathog. 114, 41–45. https://doi.org/10.1016/j.micpath.2017.11.013.
Ramalingam, V., Dhinesh, P., Sundaramahalingam, S., Rajaram, R., 2019. Green fabrication of iron oxide nanoparticles using grey mangrove Avicennia marina for antibiofilm activity and in vitro toxicity. Surf. Interfaces 15, 70–77. https://doi.org/10.1016/j.surfin.2019.01.008.
S, G., H, J.W., K, E.S., P, J.H., K, J.-H., 2015. Reduction of graphene oxide by resveratrol: a novel and simple biological method for the synthesis of an effective anticancer nanotherapeutic molecule. Int. J. Nanomed. 10, 2951–2969. https://doi.org/10.2147/IJN.S79879.
Sachdev, A., Gopinath, P., 2015. Green synthesis of multifunctional carbon dots from coriander leaves and their potential application as antioxidants, sensors and bioimaging agents. Analyst 140, 4260–4269. https://doi.org/10.1039/c5an00454c.
Sampathkumar, Banupriya, Krishnamoorthy, Kavithaa, P.R.P., Sumathi, S., 2016. Characterisation of anethole coated iron oxide nanoparticles and assessment of its biological activity. Eur. J. Biomed. Pharm. Sci. 3, 272–278.
Schröfel, A., Kratošová, G., Šafařík, I., Šafaříková, M., Raška, I., Shor, L.M., 2014. Applications of biosynthesized metallic nanoparticles - a review. Acta Biomater. 10, 4023–4042. https://doi.org/10.1016/j.actbio.2014.05.022.
Seil, J.T., Webster, T.J., 2012. Antimicrobial applications of nanotechnology: methods and literature the need for novel antibiotics. Int. J. Nanomed. 7, 2767–2781. https://doi.org/10.2147/IJN.S24805.
Sekar, A.D., Muthukumar, H., Chandrasekaran, N.I., Matheswaran, M., 2018. Photocatalytic degradation of naphthalene using calcined Fe e ZnO/PVA nano fibers. Chemosphere 205, 610–617. https://doi.org/10.1016/j.chemosphere.2018.04.131.
Shahwan, T., Abu Sirriah, S., Nairat, M., Boyaci, E., Eroğlu, A.E., Scott, T.B., Hallam, K.R., 2011. Green synthesis of iron nanoparticles and their application as a Fenton-like catalyst for the degradation of aqueous cationic and anionic dyes. Chem. Eng. J. 172, 258–266. https://doi.org/10.1016/j.cej.2011.05.103.
Shanmuganathan, R., MubarakAli, D., Prabakar, D., Muthukumar, H., Thajuddin, N., Kumar, S.S., Pugazhendhi, A., 2018. An enhancement of antimicrobial efficacy of biogenic and ceftriaxone-conjugated silver nanoparticles: green approach. Environ. Sci. Pollut. Res. 25, 10362–10370. https://doi.org/10.1007/s11356-017-9367-9.
Sharma, B.K., Saha, A., Rahaman, L., Bhattacharjee, S., Tribedi, P., 2015. Silver Inhibits the Biofilm Formation of <i>Pseudomonas aeruginosa</i&gt. Adv. Microbiol. 05, 677–685. https://doi.org/10.4236/aim.2015.510070.
Sukumar, U.K., Packirisamy, G., 2015. Bioactive core-shell nanofiber hybrid scaffold for efficient suicide gene transfection and subsequent time resolved delivery of prodrug for anticancer therapy. ACS Appl. Mater. Interfaces 7, 18717–18731. https://doi.org/10.1021/acsami.5b05280.
Suresh, A.K., Pelletier, D.A., Wang, W., Morrell-Falvey, J.L., Gu, B., Doktycz, M.J., 2012. Cytotoxicity induced by engineered silver nanocrystallites is dependent on surface coatings and cell types. Langmuir 28, 2727–2735. https://doi.org/10.1021/la2042058.
Venkateswarlu, S., Rao, Y.S., Balaji, T., Prathima, B., Jyothi, N.V.V., 2013. Biogenic synthesis of Fe3O4 magnetic nanoparticles using plantain peel extract. Mater. Lett. 100, 241–244. https://doi.org/10.1016/j.matlet.2013.03.018.
Vidic, J., Stankic, S., Haque, F., Ciric, D., Le Goffic, R., Vidy, A., Jupille, J., Delmas, B., 2013. Selective antibacterial effects of mixed ZnMgO nanoparticles. J. Nanoparticle Res. 15. https://doi.org/10.1007/s11051-013-1595-4.
Vivek, R., Thangam, R., Muthuchelian, K., Gunasekaran, P., Kaveri, K., Kannan, S., 2012. Green biosynthesis of silver nanoparticles from Annona squamosa leaf extract and its in vitro cytotoxic effect on MCF-7 cells. Process Biochem. 47, 2405–2410. In: https://doi.org/10.1016/j.procbio.2012.09.025.
Wahajuddin, A.S., 2012. Superparamagnetic iron oxide nanoparticles: magnetic nanoplatforms as drug carriers. Int. J. Nanomed. 3445–3471.
Wang, H., Burgess, R.M., Cantwell, M.G., Portis, L.M., Perron, M.M., Wu, F., Ho, K.T., 2014. Stability and aggregation of silver and titanium dioxide nanoparticles in seawater: role of salinity and dissolved organic carbon. Environ. Toxicol. Chem. 33, 1023–1029. https://doi.org/10.1002/etc.2529.
Xia, T., Zhao, Y., Sager, T., George, S., Pokhrel, S., Li, N., Schoenfeld, D., Meng, H., Lin, S., Wang, X., Wang, M., Ji, Z., Zink, J.I., Mädler, L., Castranova, V., Lin, S., Nel, A.E., 2011. Decreased dissolution of ZnO by iron doping yields nanoparticles with reduced toxicity in the rodent lung and zebrafish embryos. ACS Nano 5, 1223–1235. https://doi.org/10.1021/nn1028482.